The Astrophysical Journal, 869:171 (16pp), 2018 December 20 https://doi.org/10.3847/1538-4357/aaf007

Chandra Observations of *NuSTAR* Serendipitous Sources near the Galactic Plane

John A. Tomsick[1], George B. Lansbury[2], Farid Rahoui[3], James Aird[2], David M. Alexander[4], Maïca Clavel[5], AnaSofija Cuturilo[6], Francesca M. Fornasini[7], JaeSub Hong[7], Lizelke Klindt[4], and Daniel Stern[8]
[1] Space Sciences Laboratory, 7 Gauss Way, University of California, Berkeley, CA 94720-7450, USA
[2] Institute of Astronomy, University of Cambridge, Madingley Road, Cambridge CB3 0HA, UK
[3] Department of Astronomy, Harvard University, 60 Garden Street, Cambridge, MA 02138, USA
[4] Centre for Extragalactic Astronomy, Department of Physics, University of Durham, South Road, Durham DH1 3LE, UK
[5] Univ. Grenoble Alpes, CNRS, IPAG, F-38000 Grenoble, France
[6] Seattle Pacific University, 3307 3rd Ave West, Seattle, WA 98119-1997, USA
[7] Harvard-Smithsonian Center for Astrophysics, 60 Garden Street, Cambridge, MA 02138, USA
[8] Jet Propulsion Laboratory, California Institute of Technology, 4800 Oak Grove Drive, Pasadena, CA 91109, USA
Received 2018 August 6; revised 2018 November 2; accepted 2018 November 9; published 2018 December 26

Abstract

The *Nuclear Spectroscopic Telescope Array* (*NuSTAR*) serendipitous survey has already uncovered a large number of active galactic nuclei (AGNs), providing new information about the composition of the cosmic X-ray background. For AGNs off the Galactic plane, it has been possible to use existing X-ray archival data to improve source localizations, identify optical counterparts, and classify the AGNs with optical spectroscopy. However, near the Galactic plane, better X-ray positions are necessary to achieve optical or near-IR identifications due to the higher levels of source crowding. Thus, we have used observations with the *Chandra X-ray Observatory* to obtain the best possible X-ray positions. With eight observations, we have obtained coverage for 19 *NuSTAR* serendips within 12° of the plane. One or two *Chandra* sources are detected within the error circle of 15 of the serendips, and we report on these sources and search for optical counterparts. For one source (NuSTAR J202421+3350.9), we obtained a new optical spectrum and detected the presence of hydrogen emission lines. The source is Galactic, and we argue that it is likely a cataclysmic variable. For the other sources, the *Chandra* positions will enable future classifications in order to place limits on faint Galactic populations, including high-mass X-ray binaries and magnetars.

Key words: stars: black holes – stars: neutron – surveys – white dwarfs – X-rays: stars

1. Introduction

With its ability to focus hard X-rays, the *Nuclear Spectroscopic Telescope Array (NuSTAR)* provides unprecedented sensitivity above ∼10 keV Harrison et al. (2013). Thus, surveys with *NuSTAR* allow us to study faint populations of high-energy sources, including active galactic nucleus (AGN) as well as Galactic populations such as X-ray binaries, cataclysmic variables (CVs), pulsar wind nebulae, supernova remnants, and stars with active coronae. The *International Gamma-ray Astrophysics Laboratory (INTEGRAL)* satellite and the Burst Alert Telescope on the *Swift* satellite have surveyed the sky at 17–100 keV and 15–55 keV, respectively (Ajello et al. 2012; Bird et al. 2016), but *NuSTAR* is extending to flux levels that are approximately two orders of magnitude lower. For high-mass X-ray binaries (HMXBs), *INTEGRAL* has been used to constrain their surface density ($\log N - \log S$) down to $\sim 10^{-11}$ erg cm^{-2} s^{-1} (Lutovinov et al. 2013), but Tomsick et al. (2017) demonstrate the possibility of extending the constraints down below 10^{-13} erg cm^{-2} s^{-1} with *NuSTAR*.

Using *NuSTAR* data from the first 40 months of the mission, Lansbury et al. (2017, henceforth L17) carried out a search for serendipitously detected *NuSTAR* sources (i.e., serendips). L17 compiled a catalog of 497 sources in the primary source catalog and 64 sources in the secondary source catalog. As described in L17, the secondary catalog consists of sources that are robustly detected using a secondary source detection method that is different from the method used for the primary catalog. The 3–24 keV energy band was used for the serendipitous survey, and the sky coverage was ∼13 deg^2. Of the 561 sources in both the primary and secondary catalogs, optical identifications have been obtained for 318. Optical spectroscopy shows that 297 are likely AGNs and 21 are likely Galactic, but the identity of the optical counterpart is uncertain for five of these. The nature of 16 of the Galactic sources with secure counterpart identifications in the primary and secondary catalogs has been investigated (Tomsick et al. 2017), and they include stars, CVs, low-mass X-ray binaries (LMXBs), and HMXBs. In addition, at least one previously known magnetar is also among the serendips. In fact, more magnetars may be present among the unclassified serendips; however, given that most of the serendip classifications thus far have been based on optical spectra, the magnetars, which are typically very faint in the optical, would not have been found.

Tomsick et al. (2017) investigated how the completeness of source classifications depends on Galactic latitude, and while the completeness is 63% for sources in the primary catalog that are more than 10° from the Galactic plane, this drops to 32% at 5°–10°, and only seven of 57 sources (12%) have been classified at $|b| < 5°$. A major reason for the incompleteness at low Galactic latitudes is source confusion. L17 searched for X-ray counterparts for *NuSTAR* serendips with coverage by *XMM-Newton*, *Swift*, or *Chandra*, and used the X-ray positions to search for optical or near-IR (OIR) matches. They used the separations between the X-ray and OIR positions along with the sky density of OIR sources to estimate the spurious matching fractions. For high-latitude sources ($|b| > 10°$) with *XMM* or *Swift* positions, the spurious matching fractions were 6%–16%, but they were 1.2%–1.7% for high-latitude sources with *Chandra* positions. Thus, the reliability of the L17

Table 1
Chandra Observations

ObsID	l (degree)	b (degree)	Start Time (UT)	Exposure Time (s)
17245	73.14	−2.15	2015 Nov 27, 3.26 hr	13946
17246	321.62	+6.76	2015 Jun 12, 16.04 hr	4939
17247	10.29	+11.17	2015 Feb 24, 16.15 hr	4952
17248	10.35	+11.27	2015 Feb 14, 9.56 hr	5954
17704	73.12	−2.10	2015 Jul 25, 18.68 hr	28755
18087	304.25	−0.96	2016 May 3, 10.42 hr	9956
18088	62.11	−9.39	2016 May 2, 16.42 hr	9943
18089	80.27	−11.18	2016 Apr 7, 7.17 hr	19929

classifications is very high for the $|b| > 10^{\circ}$ serendips. Although L17 did not give specific numbers for low-latitude sources, the larger OIR sky densities would naturally lead to significantly larger spurious matching fractions. Thus, we have obtained *Chandra* observations for low-latitude sources to improve the X-ray positions and find OIR counterparts.

Here, we report on *Chandra* observations obtained to attempt to identify and classify more of the *NuSTAR* serendips close to the Galactic plane. In Section 2, we describe the *Chandra* observations that we use and our analysis procedures, including source detection. Results are presented in Section 3, and our main goal is to assess whether the *Chandra* sources detected are counterparts to the *NuSTAR* serendips. We also search on-line catalogs and obtain archival optical images to determine if the *Chandra* sources have optical or near-IR counterparts. In Section 4, we discuss the results for the serendips with new *Chandra* coverage.

2. Observations and Analysis

As we are focusing on Galactic sources, these observations target *NuSTAR* serendips within 12° of the Galactic plane. Table 1 lists the *Chandra* observations that we used for this work. We obtained seven of the pointings as part of our *Chandra* Guest Observer (GO) programs from cycle 16 and 17, and these were carried out with the aimpoint (the center of the field of view) on the ACIS-S CCD chip. We also used one additional ACIS pointing (ObsID 17704) from the *Chandra* archive. These observations were all made during 2015 and 2016 with exposure times ranging from 4.9 to 28.8 ks. As we selected the *Chandra* targets before the completion of L17, the *Chandra* coverage only includes a fraction of the unclassified serendips. In the primary and secondary L17 catalogs, there are 114 sources within 12° of the Galactic plane, and 30 of them were classified in L17.

Each of the *Chandra* GO observations targeted a *NuSTAR* serendip, and the black hole transient V404 Cyg was the target of ObsID 17704. In addition to the primary target, the *Chandra* observations cover other *NuSTAR* serendips because of the similar sizes of the *Chandra* and *NuSTAR* fields of view, and Table 2 lists the 19 serendips for which *Chandra* coverage was obtained. Each serendip has a *NuSTAR* source name as well as a catalog number. Sources starting with "P" are in the primary L17 catalog, and those starting with "S" are in the secondary L17 catalog. The specific targets of the *Chandra* observations are listed in Table 3. Here, we have grouped the ObsIDs according to the six *NuSTAR* fields being covered. An example field is shown in Figure 1, where five serendips were detected by *NuSTAR* (P444, P445, P446, P447, and P448). For *Chandra* ObsID 17245, the primary target was P448, and Figure 1(b) shows that four of the five serendips were covered. We added ObsID 17704 (not shown in Figure 1) to this study since it provides coverage of the fifth serendip (P446).

To analyze the data from the *Chandra* observations, we used the *Chandra* Interactive Analysis of Observations (CIAO)

Table 2
NuSTAR Serendips Studied in This Work

NuSTAR Name	L17 Catalog Name	R.A. (J2000) (degrees)	Decl. (J2000) (degrees)
NuSTAR J145439–5135.3	P347	223.66539	−51.58938
NuSTAR J172750–1414.8	P388	261.96027	−14.24671
NuSTAR J172755–1417.4	P389	261.98068	−14.29110
NuSTAR J172803–1423.0	P390	262.01660	−14.38466
NuSTAR J172805–1416.5	P391	262.02155	−14.27610
NuSTAR J172805–1420.9	P392	262.02435	−14.34984
NuSTAR J172806–1420.3	P393	262.02646	−14.33960
NuSTAR J172807–1418.2	P394	262.03070	−14.30409
NuSTAR J172843–1419.0	P395	262.17938	−14.31705
NuSTAR J202313+2042.8	P443	305.80463	+20.71419
NuSTAR J202339+3347.7	P444	305.91287	+33.79657
NuSTAR J202351+3354.3	P445	305.96622	+33.90517
NuSTAR J202359+3348.4	P446	305.99915	+33.80822
NuSTAR J202420+3347.7	P447	306.08377	+33.79522
NuSTAR J202421+3350.9	P448	306.09122	+33.84916
NuSTAR J211935+3337.0	P463	319.89969	+33.61708
NuSTAR J130157–6358.1	S43	195.48941	−63.96994
NuSTAR J130324–6348.6	S44	195.85243	−63.81157
NuSTAR J172822–1421.4	S53	262.09515	−14.35694

Table 3
Chandra Coverage of *NuSTAR* Serendips

ObsID	Primary *Chandra* Target	Target of *NuSTAR* Field	Other Serendips Covered
17245	P448	V404 Cyg	P444, P445, P447
17704	V404 Cyg	V404 Cyg	P444, P445, P446, P447
17246	P347	IGR J14552–5133	···
17247	P392	PDS 456	P388-P391, P393-P395, S53
17248	P388	PDS 456	P389, P391, P395, S53
18087	S44	PSR B1259–63	S43
18088	P443	Nova Del 2013	···
18089	P463	2MASX J21192912 +3332566	–

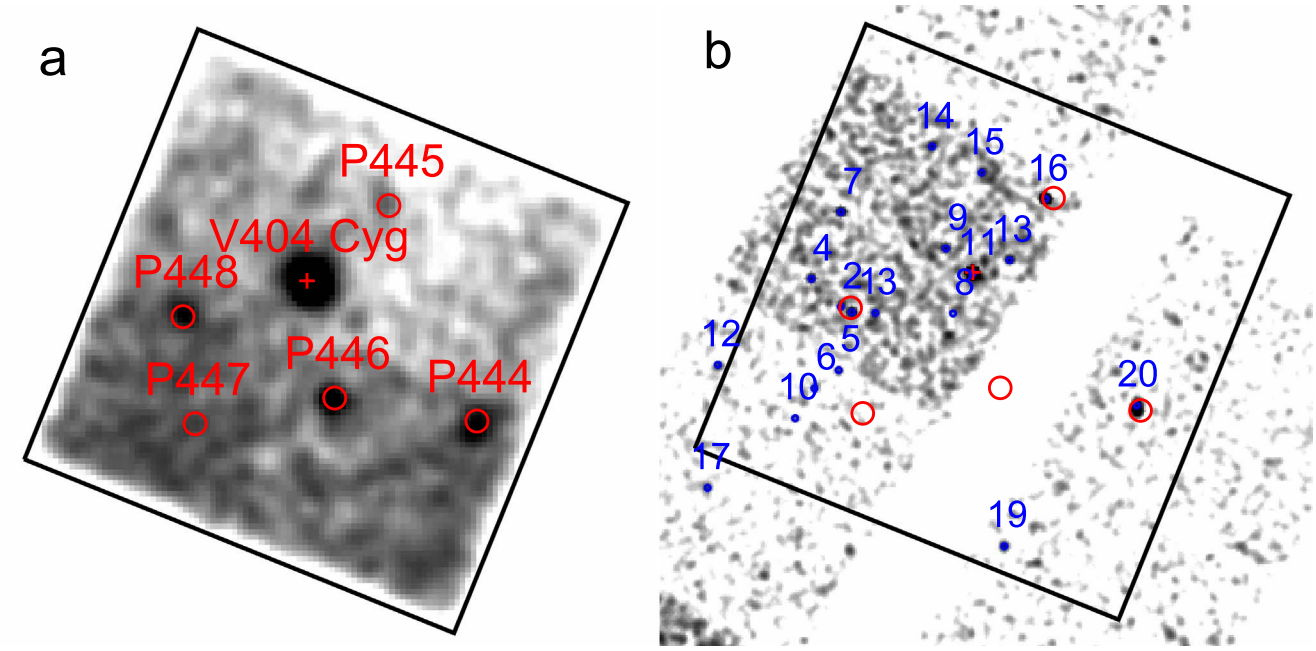

Figure 1. (a) 3–24 keV *NuSTAR* image for focal plane module A from ObsID 30001010003 with an exposure time of 97 ks. The primary target of the observation was the black hole transient V404 Cyg (marked with a red "+"), and the observation was taken in 2013 when V404 Cyg was in quiescence. Five *NuSTAR* serendips from L17 are marked with red circles with radii of 20″. (b) 0.5–7 keV *Chandra* image from ObsID 17245. The sources detected are marked with blue circles with radii of 5″ (much larger than the actual position uncertainties). The black square shows the *NuSTAR* field of view. P446 falls in a gap between *Chandra* CCDs. These images and all the images in this work are oriented so that north is up and east is to the left.

version 4.9 software and Calibration DataBase 4.7.4. For each ObsID, we made event lists with `chandra_repro` and searched for sources using `wavdetect` (Freeman et al. 2002). We followed the source detection procedures recommended for CIAO users.[9] Using `fluximage`, we produced a 0.5–7 keV "broad" band exposure-corrected image and an exposure map for 2.3 keV photons. The size of the point-spread function (PSF) depends strongly on the off-axis angle, and we made a PSF map for an energy of 2.3 keV and an encircled energy of 0.393. We ran `wavdetect` with wavelet scales of 1, 2, 4, 8, and 16 pixels, and set the detection threshold at a level estimated to give the detection of one false source. The data for ObsID 17704 were obtained when V404 Cyg was in outburst, and the dust-scattering halo produces soft X-ray emission covering much of the ACIS field of view (Heinz et al. 2016). Therefore, for this ObsID, we used the "hard" energy band (2–7 keV) to minimize the contribution from the dust-scattering halo for this observation. As described in the Appendix, we cross-correlated the positions of the detected *Chandra* sources with those in several OIR source catalogs (e.g., *Gaia*). Where possible, we used the optical or IR positions to register the *Chandra* images (see the Appendix for details). However, the errors on the *Chandra* positions in this work still assume the standard value of 0.″64 (90% confidence) for the systematic component (Weisskopf 2005).

For the *Chandra* photometry, we used `mkpsfmap` to determine the 95% encircled energy radii for each source found with `wavdetect` and extracted the counts in the 0.5–2 keV, 2–7 keV, and 0.5–7 keV energy bands within the circles. We estimated the background rates by extracting counts in the same three energy bands from large source-free regions. As some of the sources were on front-illuminated CCDs while others were on back-illuminated CCDs, we determined background rates for both cases, and then subtracted the background for all sources. All of the sources with positive numbers of 0.5–7 keV source counts after background subtraction are included in Table 7.

[9] See http://cxc.harvard.edu/ciao/threads/wavdetect/.

3. Results

3.1. Chandra Candidates for NuSTAR Serendips

From the full list of *Chandra* sources (Table 7), we consider sources within 20″ of the best positions of the *NuSTAR* serendips to be potential candidates. We use 20″ as our criterion based on the fact that the 90% confidence errors on the *NuSTAR* positions range from 14″ to 22″ depending on the significance of the detection (L17). Of the 19 *NuSTAR* serendips covered by the *Chandra* observations, there are 15 with at least one *Chandra* source within 20″, and the *Chandra* sources that are candidates for being associated with the *NuSTAR* serendips are listed in Table 4. In 10 cases there are single candidates, and in the other five cases there are two candidates. Figure 2 shows the *Chandra* images, indicating that P393, P394, P443, P444, and P448 are the serendips with two candidates.

One of the serendips, S43, is the known HMXB 2RXP J130159.6–635806 (Krivonos et al. 2015). It has already been considered in the context of the Galactic populations present in the group of *NuSTAR* serendips (Tomsick et al. 2017). In the *Chandra* program, we did not specifically target it but it was serendipitously covered by the S44 pointing (see Table 3).

To determine which of the *Chandra* candidate counterparts are likely to be matches to the *NuSTAR* serendips, we have produced hardness–intensity diagrams (see Figure 3). The 0.5–7 keV count rates are simply the counts from Table 4 divided by the exposure time for the appropriate ObsID, and we determined the 0.5–2 keV and 2–7 keV rates, $r_{\rm soft}$ and $r_{\rm hard}$, in

Table 4
Chandra Candidate Matches to *NuSTAR* Serendips

Source ID[a]	CXOU Name[b]	*Chandra* R.A. (J2000, h, m, s)	*Chandra* Decl. (J2000, degree, ′, ″)	Position Error (″)[c]	ACIS Counts[d]	Serendip Number[e]
17246-1	J145440.6–513515	14 54 40.60	−51 35 15.1	0.73	11.9 ± 4.6	P347
17248-1	J172751.4–141440	17 27 51.40	−14 14 40.0	0.74	9.8 ± 4.3	P388
17247-19	···	17 27 51.45	−14 14 40.6	2.72	8.2 ± 4.1	P388
17247-4	J172804.6–142306	17 28 04.67	−14 23 06.0	0.73	33.8 ± 6.9	P390
17248-15	J172806.1–141637	17 28 06.12	−14 16 37.3	1.03	12.4 ± 4.7	P391
17247-10	···	17 28 06.17	−14 16 37.0	1.15	8.8 ± 4.1	P391
17247-1	J172805.7–142108	17 28 05.76	−14 21 08.2	0.80	4.8 ± 3.4	P392
17247-2	J172805.1–142014	17 28 05.19	−14 20 14.9	0.78	5.8 ± 3.6	P393
17247-3	J172807.1–142024	17 28 07.15	−14 20 24.6	0.77	6.8 ± 3.8	P393
17247-5	J172806.6–141828	17 28 06.64	−14 18 28.9	0.85	7.9 ± 4.0	P394
17247-6	J172807.6–141805	17 28 07.67	−14 18 05.1	1.04	4.9 ± 3.4	P394
18088-1	J202312.4+204248	20 23 12.49	+20 42 48.8	0.72	18.6 ± 5.4	P443
18088-2	J202313.7+204245	20 23 13.78	+20 42 45.3	0.72	19.5 ± 5.6	P443
17704-13	J202339.6+334800	20 23 39.67	+33 48 00.8	1.24	30.0 ± 6.9	P444
17704-16	J202339.6+334747	20 23 39.70	+33 47 47.2	1.12	42.8 ± 7.9	P444
17245-20	···	20 23 39.69	+33 47 58.9	1.64	48.1 ± 8.4	P444
17704-7	J202353.2+335418	20 23 53.23	+33 54 18.1	0.80	35.0 ± 7.1	P445
17245-16	···	20 23 53.11	+33 54 18.0	1.05	50.5 ± 8.5	P445
17704-5	J202400.3+334829	20 24 00.39	+33 48 29.3	0.77	41.4 ± 7.6	P446
17245-1	J202421.6+335050	20 24 21.69	+33 50 50.3	0.72	15.4 ± 5.1	P448
17245-2	J202423.3+335100	20 24 23.33	+33 51 00.3	0.76	7.5 ± 4.0	P448
18089-1	J211935.5+333644	21 19 35.52	+33 36 44.0	0.75	8.2 ± 4.1	P463
18087-17	J130158.6–635807	13 01 58.66	−63 58 07.5	0.97	4141.4 ± 65.6	S43
17247-12	J172822.7–142124	17 28 22.78	−14 21 24.9	1.18	8.6 ± 4.1	S53
17248-28	···	17 28 22.70	−14 21 25.7	4.22	17.1 ± 5.7	S53

Notes.
[a] The sources are identified by ObsID and the *Chandra* source number from the full source list (Table 7).
[b] The naming convention for unregistered *Chandra* sources is for their names to start with CXOU (see http://cxc.cfa.harvard.edu/cdo/scipubs.html).
[c] The 90% confidence uncertainty on the position, including statistical and systematic contributions.
[d] The number of ACIS counts detected (after background subtraction) in the 0.5–7 keV band (except for ObsID 17704, for which the energy band is 2–7 keV). The errors are 68% confidence Poisson errors using the analytical approximations from Gehrels (1986).
[e] If the *Chandra* source falls within the error circle of a *NuSTAR* serendipitous source, then this indicates the number of the *NuSTAR* serendipitous source in the L17 catalog.

the same manner. The hardness is defined as the ratio of $r_{\rm hard}$–$r_{\rm soft}$ over $r_{\rm hard}$+$r_{\rm soft}$; thus, a source with all of its counts in the 2–7 keV band will have a hardness of +1.0, and a source with all of its counts in the 0.5–2 keV band will have a hardness of −1.0. Sources which will contribute significantly to the 3–24 keV fluxes detected by *NuSTAR* are expected to occupy the harder and/or higher count rate parts of the plots unless they have significant variability. For sources detected in multiple ObsIDs, we calculated weighted averages of the rates and the hardness ratios, and these are plotted in Figure 3.

Figure 3(a) shows the hardness–intensity diagrams for the serendips with single *Chandra* candidates. Indeed, nine of the 10 sources have either high count rates or hard spectra. Of the nine, P391 is the most marginal, but the *Chandra* position confirms the match with the optical source that has previously been classified as an AGN based on its optical spectrum, providing a reason to think that the *Chandra* candidate is likely to be the correct counterpart. The *Chandra* candidate for P463 is a very soft source with the lowest count rate in the group, and we suspect that it (18089-1) may not be associated with P463. Although Figure 2 shows two possible candidates for P444 (17704-13 and 17704-16), the contamination from the V404 Cyg X-ray halo in ObsID 17704 does not allow for a determination of the hardness for these two sources. Thus, for P444, Figure 3(a) shows the count rate and hardness for 17245-20, which is a blend of 17704-13 and 17704-16. It is currently unclear whether P444 is a combination of emission from two point sources or if there is a single extended source. The HMXB S43 has a 0.5–7 keV rate of 0.410 ± 0.007 c/s (outside the range of the plots) and a hardness of 0.75 ± 0.02 (1σ errors).

Figures 3(b), (c), and (d) provide the values for the serendips with two *Chandra* candidate counterparts. While the *NuSTAR* flux for these serendips (P393, P394, P443, and P448) may include contributions from both *Chandra* sources, the plots suggest that 17247-3, 17247-6, 18088-1, and 17245-1 are

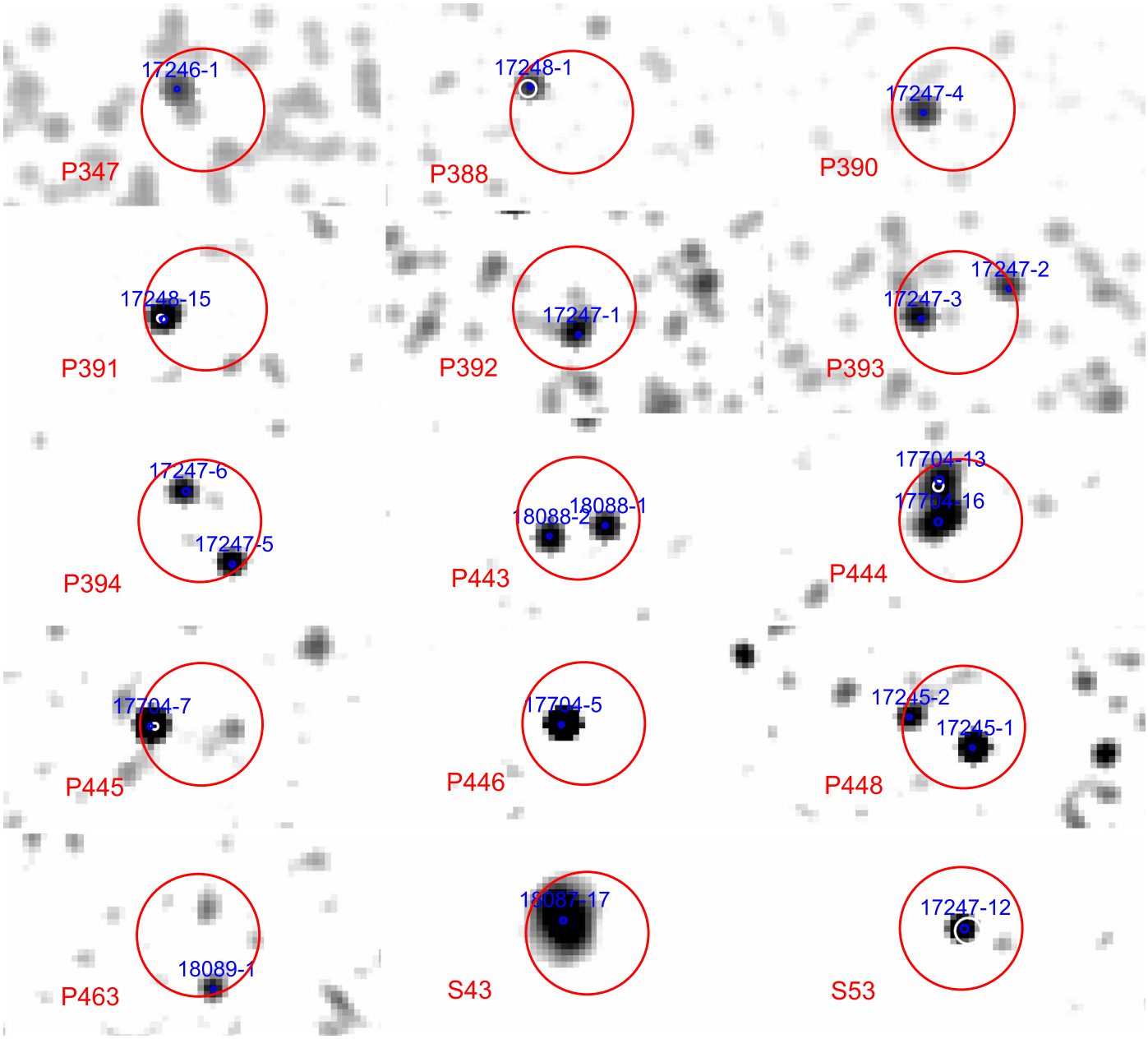

Figure 2. *Chandra* images for the sources in Table 4. The 20″ *NuSTAR* error circles are shown in red. The *Chandra* sources are marked with blue or white circles with radii equal to the position uncertainty. The blue circles are labeled with the *Chandra* source names, and these also indicate which ObsIDs are used to make the images. The white circles are for sources detected in more than one ObsID (17247-19 for P388, 17247-10 for P391, 17245-20 for P444, 17245-16 for P445, and 17248-28 for S53). The energy band is 0.5–7 keV except for ObsID 17704 (P444, P445, and P446) where 2–7 keV is used.

likely to contribute more to the fluxes of their respective *NuSTAR* serendips as they are the harder sources. However, we note that the error bars overlap in all four cases, so this is not a strong conclusion.

The four serendips without *Chandra* detections are P389, P395, P447, and S44. In the first three cases, there are no *Chandra* sources even within an arcminute, indicating *Chandra* non-detections for P389, P395, and P447. Explanations for the non-detections could be source variability or possibly that some of the *NuSTAR* detections are spurious. For S44, there are two *Chandra* sources that are 35″ away from the *NuSTAR* position. The angular separation is too large to consider these as likely candidates, but we mention them as possible candidates.

L17 used soft X-ray data, primarily from archives, to search for counterparts in the *NuSTAR* error circles of the serendips. For the 19 serendips that we are studying in this work, *XMM-Newton* sources were found in 13 cases, *Chandra* sources were found in two cases (P347 and S53), a *Swift* X-ray telescope source was found in one case (P443), and there were case serendips with no soft X-ray counterparts (P389, P447, and P463). The new *Chandra* positions that we are reporting here (Table 4) are a significant improvement over those of *XMM* and *Swift* because of *Chandra*'s superior angular resolution. For the two serendips that already had *Chandra* positions, we compared the new positions to the X-ray positions given in L17. For P347 and S53, the differences in position are 0.″20 and 0.″86, respectively. For

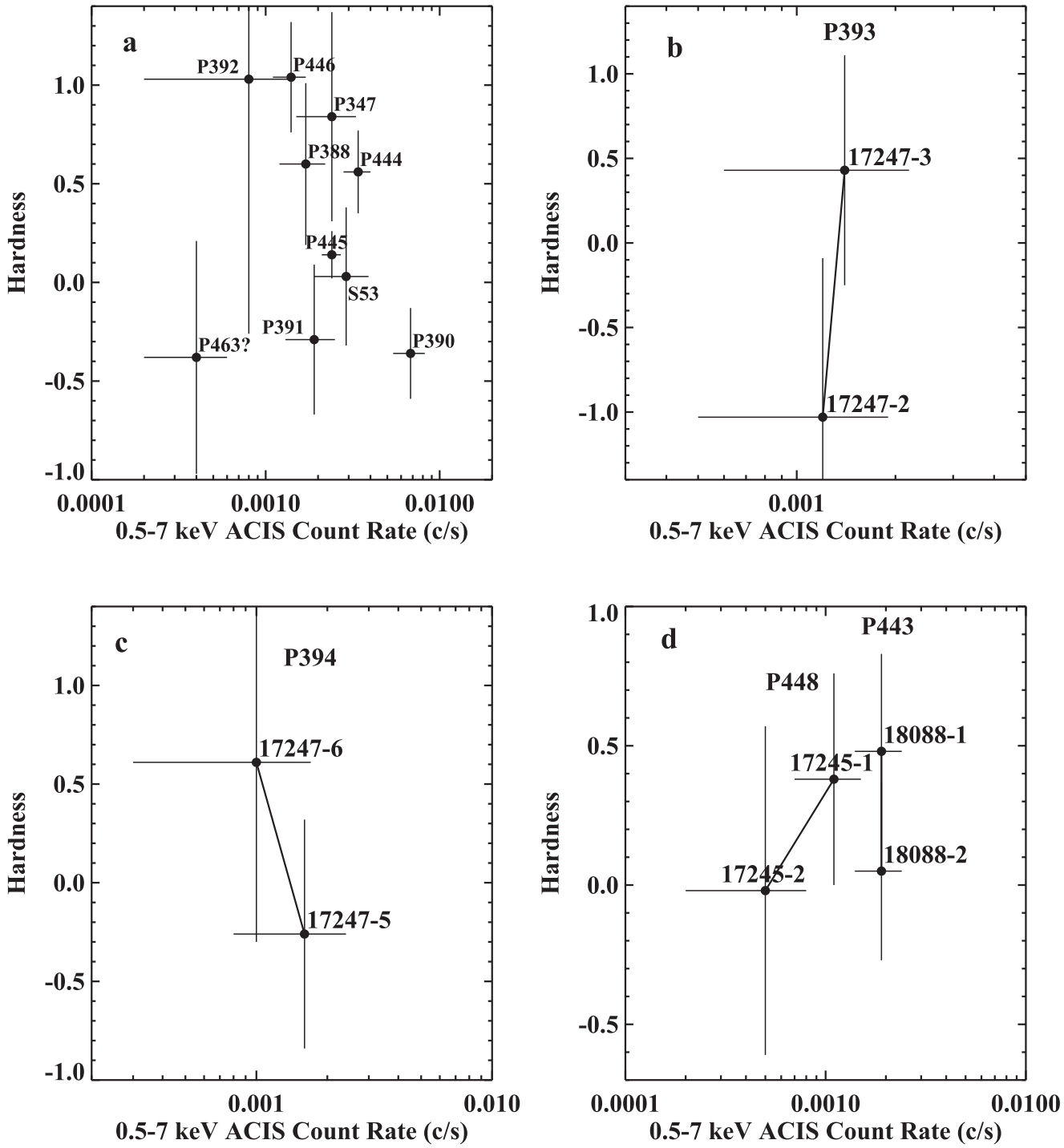

Figure 3. Hardness–intensity diagram using 0.5–7 keV, 0.5–2 keV ($=r_{\rm soft}$), and 2–7 keV ($=r_{\rm hard}$) *Chandra*/ACIS count rates. The hardness is defined as $(r_{\rm hard}-r_{\rm soft})/(r_{\rm hard}+r_{\rm soft})$. The errors bars are 1σ errors using the Gehrels approximation for Poisson statistics.

P347, the difference is considerably smaller than the position uncertainty. For S53, the difference is likely due to the fact that we have registered the images for the careful analysis carried out in this work (see the Appendix).

3.2. Optical Counterparts

The *Chandra* positions allow us to check on the optical counterparts that were suggested in L17 based mostly on *XMM* positions. In many cases, optical spectroscopy was performed, and the sources have been classified. Of the 15 serendips listed in Table 4, eight of them have candidate OIR counterparts in L17. The separations between the *Chandra* positions and the L17 OIR positions are given in Table 5. For P347, P388, P390, and P391, the *Chandra* positions confirm the optical candidates. In these cases, the *Chandra* positions are consistent with the optical positions with separations of $0\farcs38 \pm 0\farcs73$, $0\farcs29 \pm 0\farcs74$, $0\farcs31 \pm 0\farcs73$, and $0\farcs30 \pm 1\farcs15$ (90% confidence errors, including statistical and systematic contributions) for the four sources, respectively. All four of these sources have been optically classified as AGNs.

Table 5
NuSTAR Serendips with Optical or Near-IR Positions in L17

Serendip ID	*Chandra* Sources	Separation between *Chandra* and L17 (arcsec)[a]	L17 Classification
Confirmations			
P347	17246-1	0.38 ± 0.73	AGN
P388	17248-1	0.29 ± 0.74	AGN
	17247-19	0.78 ± 2.72	"
P390	17247-4	0.31 ± 0.73	AGN
P391	17247-10	0.30 ± 1.15	AGN
	17248-15	0.76 ± 1.03	"
Non-confirmations			
P392	17247-1	1.59 ± 0.80	AGN
P448	17245-1	2.23 ± 0.72	?
	17245-2	24.93 ± 0.76	"
P463	18089-1	24.37 ± 0.75	?
S53	17247-12	4.10 ± 1.18	AGN
	17248-28	2.91 ± 4.22	"

Note.
[a] The 90% confidence uncertainty on the position, including statistical and systematic contributions.

The *Chandra* positions for P392, P448, P463, and S53 are significantly offset from the optical positions listed in L17 (see Table 5). Figure 4 shows archival optical (*i*-band) images covering the *NuSTAR* error regions for these four serendips. For P392, the *Chandra* source is $1\farcs59 \pm 0\farcs80$ from the L17 position, which is based on the position of a USNO-B1.0 optical source with $I = 15.6$ that is inside the *NuSTAR* error circle as well as being inside the error circle of an *XMM-Newton* source. While the VizieR database does not have any optical sources with positions that are consistent with the *Chandra* position, the USNO-B1.0 source position is within $1\farcs6$. The SDSS optical image (Figure 4(a)) suggests that the USNO-B1.0 source is actually a blend of optical sources, and the *Chandra* position shows that the correct P392 counterpart is the fainter source to the northeast. L17 obtained an optical spectrum targeting the position of the USNO-B1.0 source and classified P392 as an AGN with a redshift of $z = 0.197$, but there is uncertainty as to which of the narrowly offset optical sources corresponds to the AGN.

For P448, the L17 serendip catalog indicated that there is uncertainty about the optical counterpart. The L17 optical position identifies a unique optical source, but the *Chandra* position indicates that a different optical source is the actual counterpart. This is due to the deeper optical imaging being used here. A search of the VizieR database shows that the optical counterpart for P448 is in the IPHAS catalog with a brightness of $i = 19.56 \pm 0.10$, and we performed follow-up optical spectroscopy of this source (see Section 4). For P463, there is no evidence for X-rays from the L17 optical source, and the only *Chandra* candidate counterpart does not have an optical counterpart. For S53, there is an optical source consistent with the *Chandra* position (Figure 4(d)). Although S53 does not appear in any optical catalogs in the VizieR database, there is a *WISE* source within $0\farcs61$ of the *Chandra* position for S53. Specifically, WISE J172822.82–142124.7 has magnitudes of $m_{3.35\ \mu m} = 15.16 \pm 0.04$, $m_{4.6\ \mu m} = 14.56 \pm 0.06$, and $m_{11.6\ \mu m} = 11.71 \pm 0.25$.

Sources P393, P394, P443, P444, P445, and P446 do not have optical counterparts listed in L17. We searched the catalogs in the VizieR database for any optical or IR sources consistent with the positions of the *Chandra* sources detected in the *NuSTAR* error circles of these serendips, and we also show the *i*-band images for these six sources in Figure 5. With one exception, the VizieR searches did not uncover likely optical or IR counterparts. For 17247-3, which is the most likely counterpart to P393, 2MASS J17280709–1420245 is a near-IR source within $0\farcs78$ of the *Chandra* position with magnitudes of $J = 16.30 \pm 0.14$ and $K_s = 15.47 \pm 0.18$. The fact that the *Chandra* position uncertainty is $0\farcs77$ indicates that the 2MASS source is at the edge of the error circle, and this can also be seen in the *i*-band image from the SDSS (Figure 5(a)). For P394, Figure 5(b) shows that there is an *i*-band source relatively close to the *Chandra* source 17247-5, but its *Gaia* position is $1\farcs5$ from the *Chandra* position, making the association unlikely. For the other *Chandra* sources in the P394, P443, P444, and P446 fields, there are no candidate counterparts in the VizieR database or in the *i*-band images (Figures 5(b), (c), (d), (f)). However, there may be an *i*-band counterpart for the *Chandra* source associated with P445. Figure 5(e) shows the PanSTARRS *i*-band image, and this is a case where the same *Chandra* source was detected in two ObsIDs (17704 and 17245), but the *Chandra* error circles just barely overlap. The *i*-band source is in the middle of the 17245-16 error circle, but it is on the edge (or maybe just outside) of the 17704-7 error circle. In all, the *i*-band and *Chandra* positions may be consistent, and we consider the *i*-band source to be a potential counterpart to P445.

Although a more detailed discussion of the results is presented in Section 5, here we provide a brief summary of the status of optical counterparts after using the information learned from the *Chandra* positions. In five cases, the *Chandra* positions are consistent with the OIR positions reported in L17: P347, P388, P390, and P391 are AGNs, and S43 is an HMXB. In three cases (P392, P448, and S53), the *Chandra* positions clearly identify the optical counterpart. Finally, in two cases (P393 and P445), there are candidate optical counterparts.

4. Optical Follow-up

We obtained optical spectra for two of the sources with newly identified counterparts (P448 and P445). For P448, the optical counterpart to *Chandra* source 17245-1 is clear (see Figure 4(b)), the magnitude is $i = 19.56 \pm 0.10$, and the name of the optical source is IPHAS J202421.67+335050.1. We took the optical spectrum at Keck Observatory with the Low Resolution Imaging Spectrometer (LRIS) on 2018 May 11 with an exposure time of 1800 s. After reducing the spectrum, we dereddened it based on the Galactic extinction along the line of sight to the source of $N_{\rm H} = 6.6 \times 10^{21}$ cm^{-2} (Kalberla et al. 2005), which corresponds to $A_V = 3.0$ (Güver & Özel 2009), and the spectrum is shown in Figure 6(a). We detect Hα, Hβ, and Paschen series emission lines at zero redshift, indicating that P448 is a Galactic source. Table 6 provides the detailed line properties for Hα and Hβ taken from the optical spectrum before dereddening. We discuss the nature of the source, considering the optical and X-ray properties in Section 5.2.

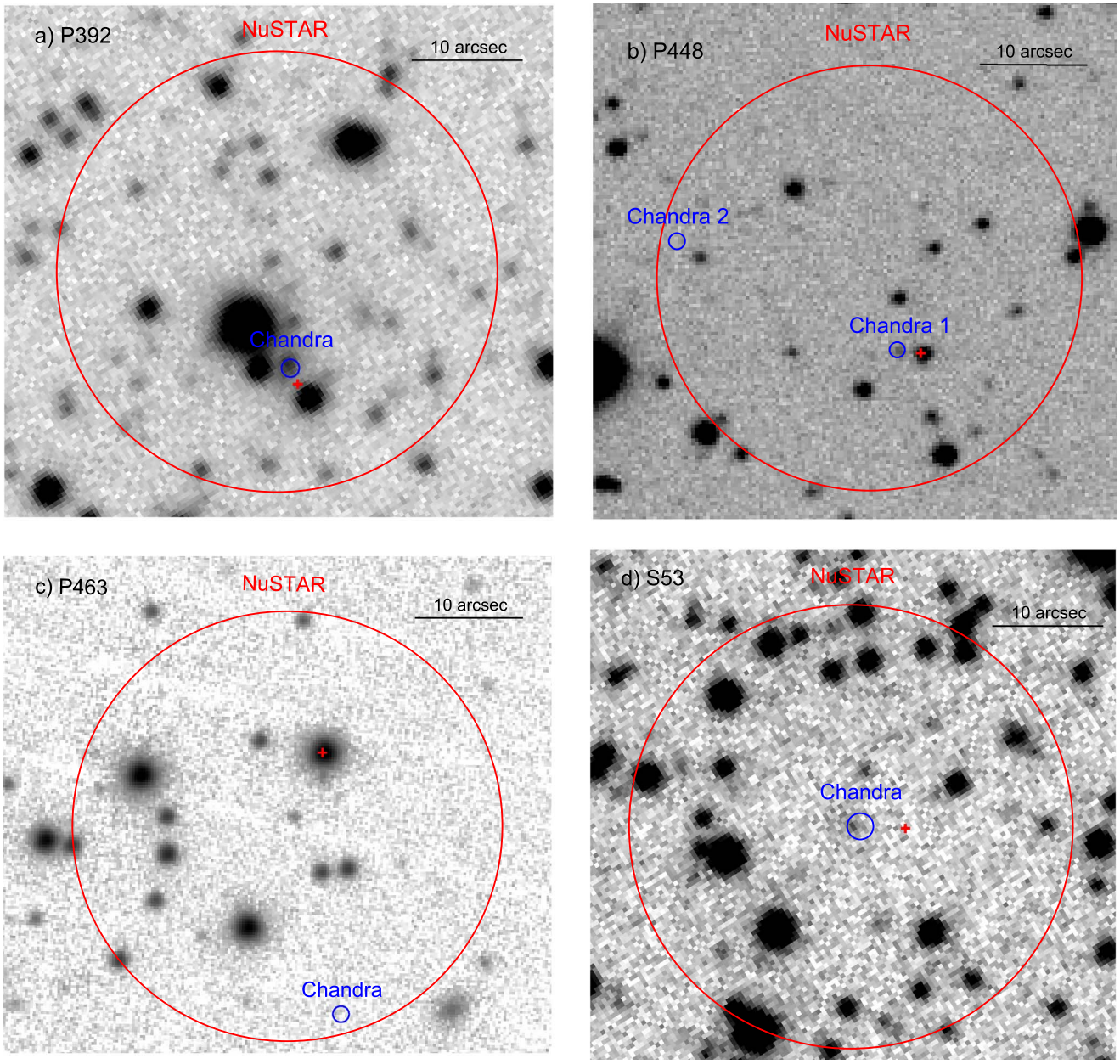

Figure 4. Optical images for the cases where the *Chandra* positions do not confirm the optical positions provided in L17. The *i*-band images come from the Sloan Digitized Sky Survey ((a) and (d)), the IPHAS survey (b), and PanSTARRS (c). The red "+" symbols mark the optical positions given in L17, and the blue circles show the locations of X-ray sources detected by *Chandra*.

We also used Keck/LRIS to observe a very faint *i*-band source that may be the counterpart to P445. The observation occurred on 2017 September 16 with an exposure time of 1800 s. As described above, the optical source is just outside the *Chandra* error circle for 17704-7 (see Figure 5(e)), but it is coincident with 17245-16. The LRIS spectrum is shown in Figure 6(b). While we detect a somewhat reddened continuum, the signal-to-noise is too poor to conclude on whether there are any emission or absorption lines, and it is not possible to classify the source or even to say whether it is Galactic or extragalactic.

5. Discussion

Here, we discuss the results that we have obtained for 19 *NuSTAR* serendips within 12° of the Galactic plane, using *Chandra* observations, archival optical observations, OIR catalog information, and follow-up optical spectroscopy. We discuss the sources in the following groupings: 1. confirmations of previous classifications; 2. sources with *Chandra* detections and a possible OIR counterpart; 3. sources with *Chandra* detections but no detected OIR counterpart; and 4. sources without *Chandra* detections.

5.1. Group 1: Confirmations (P347, P388, P390, P391, and S43)

The first four of these sources are AGNs, and S43 is the HMXB 2RXP J130159.6–635806 (Krivonos et al. 2015). The *Chandra* positions confirm the classifications. For the AGNs, the *Chandra* sources with the best positions are 17246-1, 17248-1, 17247-4, and 17248-15, respectively (see Table 4).

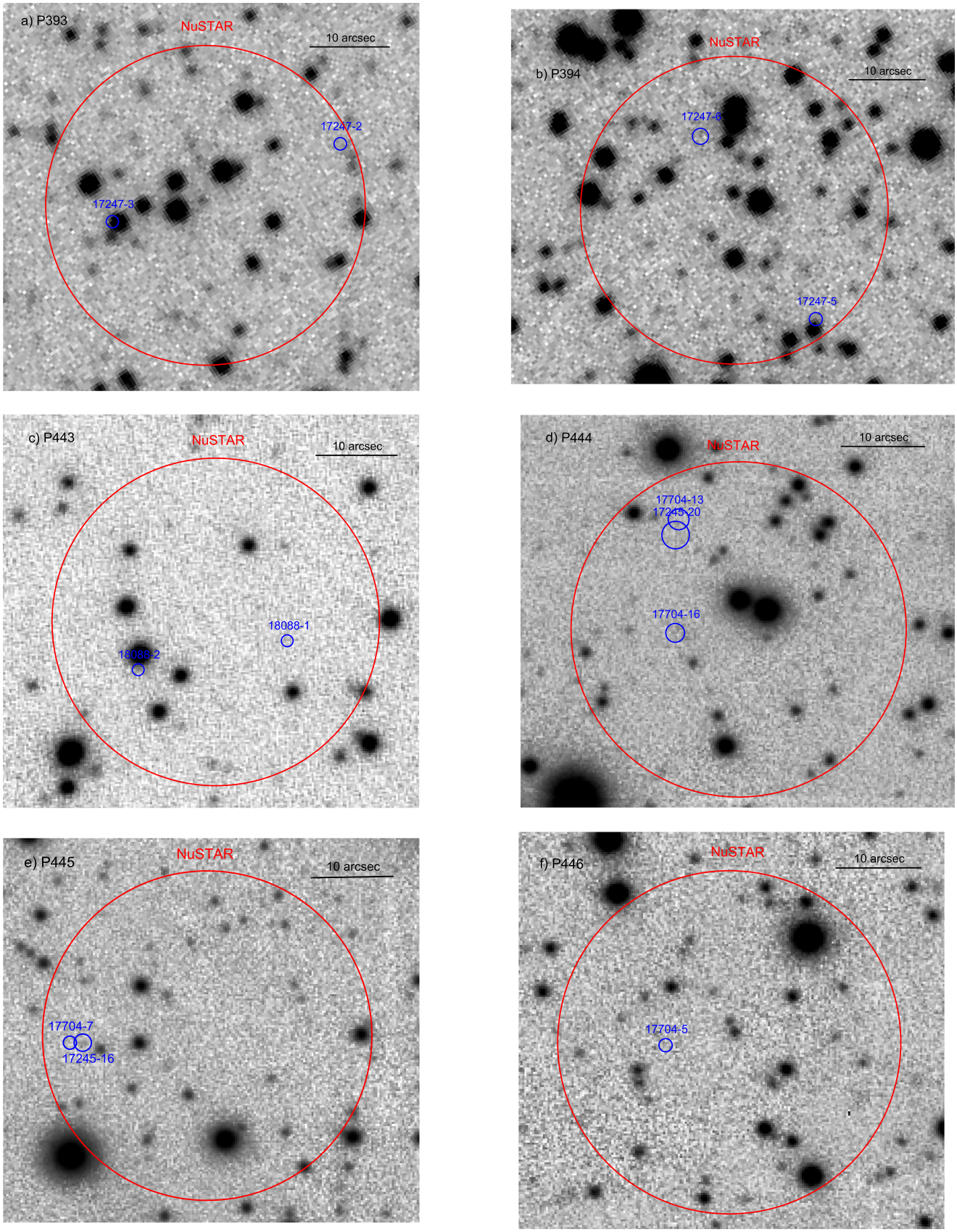

Figure 5. *i*-band images for the six sources with *Chandra* detections but no optical counterpart listed in L17. The images come from the Sloan Digitized Sky Survey ((a) and (b)) and PanSTARRS ((c), (d), (e), and (f)). The blue circles show the locations of X-ray sources detected by *Chandra*.

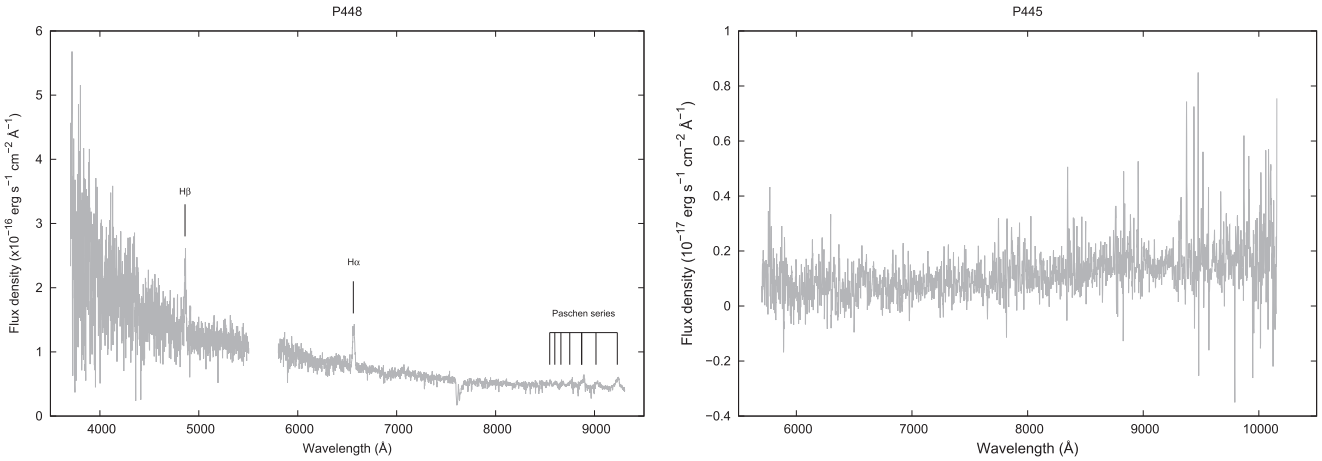

Figure 6. Left: dereddened optical spectrum for P448 (NuSTAR J202421+3350.9), which we identify with the optical source IPHAS J202421.67+335050.1. Right: optical spectrum (not dereddened) for a possible optical counterpart to P445. The signal-to-noise for the P445 spectrum is not sufficient to detect any emission or absorption lines. Both spectra are from the LRIS instrument at Keck Observatory.

Table 6
Optical Emission Lines for P448

Line[a]	Wavelength (Å)	EW[b] (Å)	FWHM[c] (km s^{-1})	Flux[b] (10^{-17} erg cm^{-2} s^{-1})
Hβ	4859 ± 0.6	14.2 ± 1.3	949 ± 43	7.0 ± 0.9
Hα	6561 ± 0.3	20.1 ± 1.7	1057 ± 14	18.89 ± 0.08

Notes.
[a] These are from the Keck/LRIS measurements of IPHAS J202421.67 +335050.1, which is the optical counterpart of CXOU J202421.6+335050.
[b] The equivalent width and the flux values are measured before dereddening.
[c] Corrected for the instrumental resolution of 215 km s^{-1} at Hα and 248 km s^{-1} at Hβ.

With these confirmations, the classification work on these sources should be complete.

5.2. *Group 2:* Chandra *and OIR (P392, P393, P445, P448, and S53)*

For P392, L17 show an optical spectrum that is clearly an AGN with $z = 0.197$; however, the optical coordinates given by L17 are offset by $1\farcs59 \pm 0\farcs80$ from the *Chandra* position for 17247-1. Given the fact that the P392 field is crowded, and we cannot confirm that the correct counterpart was targeted, it would be advisable to obtain another optical spectrum to confirm the AGN classification.

For P393, the most likely *Chandra* counterpart is 17247-3, and a possible OIR identification is 2MASS J17280709–1420245. Although the *Chandra* and 2MASS sources are separated by $0\farcs78 \pm 0\farcs77$, and the identification is not certain, we suggest that it would be worthwhile to obtain an optical or near-IR spectrum of the 2MASS source before obtaining a deeper image to look for other potential counterparts. The 2MASS magnitudes are $J = 16.30 \pm 0.14$ and $K_s = 15.47 \pm 0.18$, so obtaining a spectrum would not require a major effort.

We have a candidate optical counterpart for P445, and we obtained an optical spectrum. This has a low signal-to-noise, and we were not able to classify the source. Two possible next steps would be to obtain a higher-quality optical spectrum or to obtain a deeper near-IR image to search for other possible counterparts.

For P448, we were successful in identifying a unique optical counterpart and obtaining an optical spectrum showing that this serendip is Galactic with optical emission lines. P448 is among the group of serendips that are high priority for obtaining classifications to constrain the population of faint HMXBs (Tomsick et al. 2017). P448 is detected in the 8–24 keV bandpass (L17), and, at $b = -2\fdg1$, it is within 5° of the Galactic plane. The presence of Hα and Hβ in emission would be expected if P448 was an HMXB (e.g., a Be X-ray binary), and we have considered this possibility. If the source is a binary with a B-type companion, it would be brighter than $M_V = -0.25$ and $M_I = -0.13$ (Cox 2000). For the extinction used in Section 4 ($A_V = 3.0$), $A_I = 1.44$, and the observed magnitude ($i = 19.56$) implies a distance of 45 kpc. A much higher extinction can be ruled out by the optical spectrum. Thus, an HMXB can also be ruled out because such a large distance would put the source outside of the Galaxy.

Although an HMXB is ruled out, with the optical emission lines, possibilities for the nature of P448 include an LMXB or a CV. The *NuSTAR* spectrum is consistent with being a relatively hard power law with a photon index of $\Gamma = 1.7^{+0.4}_{-0.3}$, which does not clearly distinguish between the two possibilities. The Hα FWHM of 1057 ± 14 km s^{-1} (see Table 6) also does not provide a clear distinction, but it does favor a CV nature because LMXBs typically have broader lines (Casares 2015). If P448 is a CV, one would expect it to have an absolute magnitude in the range $M_V = 4$–11 (Patterson 1998). If we assume $M_I \sim 7$ and $A_I = 1.44$, we derive a distance of ∼2 kpc. Given the *NuSTAR* flux of 9×10^{-14} erg cm^{-2} s^{-1} (3–24 keV), we calculate a luminosity of 4×10^{31} erg s^{-1}, which is also consistent with the source being a CV.

L17 show an optical spectrum for S53, which is an AGN with $z = 0.688$. Although the optical coordinates given in L17 do not match 17247-12, we found an error in the optical coordinates, in this exceptional case. The coordinates given were the *Magellan* telescope pointing coordinates. We have checked that the position of the slit used to take the optical spectrum matches the *Chandra* position, and we can consider the AGN classification of S53 to be correct.

5.3. Group 3: Chandra but No OIR (P394, P443, P444, P446, and P463)

P394 and P443 both have two possible *Chandra* counterparts. For P394, 17247-6 may have a harder spectrum, but the errors are large. Also, 17247-5 is slightly brighter. The true *NuSTAR* serendip may be either of these sources or possibly a combination of the two. Neither of these sources has optical counterparts, and deeper near-IR observations are required for identifications.

P444 may also have two *Chandra* counterparts; however, they are not clearly resolved, and P444 may possibly be a single extended source. Given the hardness of the source, a pulsar wind nebula (PWN) is a possibility. The fact that the source or sources do not have optical counterparts is consistent with a PWN nature, but this does not constitute proof. P444 is 7′ off-axis in *Chandra* ObsID 17704 and 9′ off-axis in ObsID 17245; thus, the smearing of the PSF complicates an assessment of whether the source is extended or not. A dedicated *Chandra* observation with the source on-axis may be the next step toward classifying P444.

P446 has a unique *Chandra* counterpart, 17704-5, which has a hard spectrum (all ∼40 ACIS counts in the 2–7 keV band) and is almost certainly the correct counterpart to the *NuSTAR* serendip. It would be of great interest to obtain a deeper near-IR image to look for a counterpart.

We mention that P444 may be a PWN because it may be an extended X-ray source, but it is worth mentioning that all sources with X-ray detections but no OIR counterparts should be considered to be pulsar or magnetar candidates. If deeper near-IR images do not uncover counterparts for P394, P443, P444, and P446, then the pulsar or magnetar possibility would be likely.

Although P463 also had a unique *Chandra* counterpart, 18089-1 has a low X-ray flux and a very soft X-ray spectrum. Thus, we think there is a good chance that 18089-1 is not the correct counterpart. There are a couple of possible implications: one is that the *NuSTAR* serendip may be variable, which could suggest that it is a Galactic source. The other possibility is that P463 is a spurious detection; however, this is somewhat unlikely since L17 quote a false alarm probability (FAP) in the 3–24 keV band of 2×10^{-9} for this source. L17 also quote a 3–24 keV flux of $(1.54 \pm 0.42) \times 10^{-13}$ erg cm^{-2} s^{-1} for P463. Assuming an absorbed power-law spectral shape with a column density of $N_{\rm H} = 10^{22}$ cm^{-2} and a photon index of $\Gamma = 2$, the L17 flux would be expected to produce a *Chandra* source with 167 counts. Such a bright source would have definitely been strongly detected in ObsID 18089. Comparing 167 counts to the detectability limit suggests that P463 is variable by a factor of ∼20.

5.4. Group 4: No Chandra Detection (P447, P389, P395, and S44)

The *Chandra* non-detections for these four sources leave open the same possibilities just discussed for P463: that the sources are variable or spurious. In these cases, the spurious possibility is more likely than for P463 because their FAPs are lower. For P447, P389, and P395, the FAPs are 4×10^{-7}, 5×10^{-5}, and 3×10^{-6}, respectively, and these source detections have the lowest significances of the sources in each field. While L17 did not calculate FAPs for the secondary source catalog, the flux for S44 indicates a significance of 3.3σ.

Keeping in mind that the sources may be spurious, we use the *NuSTAR* fluxes to estimate the expected number of *Chandra* counts, making the same assumptions in the calculation for P463. The 3–24 keV flux for P447 in L17 is $(3.7 \pm 1.2) \times 10^{-14}$ erg cm^{-2} s^{-1}. For P389, P395, and S44, the 3–8 keV fluxes are $(2.1 \pm 0.6) \times 10^{-14}$, $(1.8 \pm 0.7) \times 10^{-14}$, and $(4.3 \pm 1.2) \times 10^{-14}$ erg cm^{-2} s^{-1}, respectively. Among all the *Chandra* ObsIDs where these sources are covered, the predicted number of counts ranges from 11 to 58. Thus, at the flux levels measured by *NuSTAR*, these sources should have been detected in the *Chandra* observations unless they are variable (or spurious).

5.5. Status of Galactic Hard X-Ray Population Studies

In Tomsick et al. (2017), we developed a framework for constraining the faint HMXB population, using the *NuSTAR* coverage within 5° of the Galactic plane, and focusing on the sources detected in the 8–24 keV band. L17 report 8–24 keV detections for 30 serendips at $|b| < 5°$, and these sources are our highest priority for classifications. Six of the 30 serendips were classified (as 3 AGNs, an HMXB, a magnetar, and an HMXB candidate) previously, and in this work we have taken another step toward improving the completeness of classifications by classifying P448 as a likely CV and by taking the next steps toward classifying P444, P445, and P446, which are also on the high-priority list. Even if the CV classification for P448 is not completely certain, we determined that an HMXB is ruled out since an HMXB would need to be at a distance of at least 45 kpc. Although we are still far from having a complete set of classifications for the *NuSTAR* serendipitous survery sources, when we do achieve a high level of completeness, we will have significant constraints on the faint populations of HMXBs as well as other populations that are found almost exclusively at low Galactic latitude, such as magnetars.

This work made use of data from the *NuSTAR* mission, a project led by the California Institute of Technology, managed by the Jet Propulsion Laboratory, and funded by the National Aeronautics and Space Administration. We thank the *NuSTAR* Operations, Software and Calibration teams for support with the execution and analysis of these observations. This research has made use of the *NuSTAR* Data Analysis Software (NuSTARDAS) jointly developed by the ASI Science Data Center (ASDC, Italy) and the California Institute of Technology (USA). Data from *Chandra* were also used, and the work on serendipitous *NuSTAR* sources is partially funded by *Chandra* grants GO5-16154X and GO6-17135X. This work has made use of data from the European Space Agency (ESA) mission *Gaia*, processed by the *Gaia* Data Processing and Analysis Consortium (DPAC). Funding for the DPAC has been provided by national institutions, in particular the institutions participating in the *Gaia* Multilateral Agreement. This research had made use of the SIMBAD database and the VizieR catalog access tool, CDS, Strasbourg, France as well as the VISTA and *WISE* databases and publicly available images from PanSTARRS, SDSS, and IPHAS.

Appendix

For the eight *Chandra* ObsIDs listed in Table 1, we used `wavdetect` for source detection as described in Section 2. Table 7 lists all the sources that were detected with the criterion that the number of ACIS counts minus the error on the number of ACIS counts is a positive number. The number of sources detected ranged from 14 for ObsID 17246 to 47 for ObsID 18089. Table 7 gives the source number, the angular distance between the *Chandra* aimpoint and the source (θ), the *Chandra* position and uncertainty, the number of ACIS counts for each source, and notes about other identifications.

We searched several on-line catalogs (e.g., *Gaia*, *WISE*, and *VISTA*) for matches with the *Chandra* sources. If more than a few matches can be confidently found, then the *Chandra* images can be registered. We found between four and nine *Chandra*/OIR matches for ObsIDs 17247, 17248, 18088, 18089, and 18087, and performed the shifts given in Table 8. The largest shift was $0\farcs59$ for ObsID 17247. For ObsID 17245, the only match we found was with V404 Cyg. We checked that the *Chandra* position matched the known position of V404 Cyg, but we did not perform any shifts. For ObsID 17704, we did not find OIR matches, but we did have four matches with the same X-ray sources found in ObsID 17245, and we shifted the positions for ObsID 17704 based on the matches between these two ObsIDs. Although these shifts are expected to provide a decrease in the systematic position uncertainty, we were conservative and continued to use the standard value of $0\farcs64$ (90% confidence) for errors quoted in Table 7 and elsewhere in this work.

Table 7
Chandra Sources in *NuSTAR* Serendip Fields

Source Number	θ[a] ($'$)	*Chandra* R.A. (J2000, h, m, s)	*Chandra* Decl. (J2000, degree, $'$, $''$)	Position Error[b] ($''$)	ACIS Counts[c]	Other Identification[d]
			ObsID 17246			
1	0.30	14 54 40.60	−51 35 15.1	0.73	11.9 ± 4.6	P347
2	1.63	14 54 38.25	−51 33 56.0	0.77	9.9 ± 4.3	⋯
3	2.11	14 54 34.20	−51 33 43.5	0.97	3.8 ± 3.2	⋯
4	3.77	14 55 04.27	−51 33 54.7	1.03	8.8 ± 4.1	⋯
5	3.83	14 55 06.64	−51 35 50.9	1.51	3.9 ± 3.2	⋯
6	3.90	14 54 39.78	−51 31 33.8	1.25	5.7 ± 3.6	⋯
7	4.22	14 54 59.73	−51 38 39.4	0.83	30.9 ± 6.6	⋯
8	6.16	14 54 41.11	−51 29 17.4	2.51	6.2 ± 3.8	⋯
9	7.47	14 53 55.88	−51 37 29.8	4.57	5.4 ± 3.6	⋯
10	7.98	14 53 52.74	−51 37 40.4	3.41	9.2 ± 4.3	⋯
11	8.14	14 55 16.83	−51 41 32.7	6.14	5.1 ± 3.6	⋯
12	8.71	14 54 02.47	−51 29 17.3	4.06	9.8 ± 4.4	⋯
13	8.80	14 53 45.47	−51 35 43.9	5.80	6.8 ± 4.0	⋯
14	12.29	14 54 03.27	−51 24 44.8	2.38	73.8 ± 9.9	⋯
			ObsID 17247			
1	0.33	17 28 05.76	−14 21 08.2	0.83	3.8 ± 3.2	P392
2	0.64	17 28 05.19	−14 20 14.9	0.78	5.8 ± 3.6	P393
3	0.72	17 28 07.15	−14 20 24.6	0.77	6.8 ± 3.8	P393
4	2.22	17 28 04.67	−14 23 06.0	0.73	33.8 ± 6.9	P390
5	2.44	17 28 06.64	−14 18 28.9	0.85	7.9 ± 4.0	P394
6	2.87	17 28 07.67	−14 18 05.1	1.04	4.9 ± 3.4	P394
7	3.51	17 27 51.15	−14 21 58.4	1.39	3.7 ± 3.2	*Gaia*
8	3.76	17 28 18.57	−14 22 40.4	1.21	5.7 ± 3.6	⋯
9	3.99	17 27 49.45	−14 22 15.5	1.08	8.7 ± 4.1	*Gaia*
10	4.28	17 28 06.17	−14 16 37.0	1.15	8.8 ± 4.1	*Gaia*, P391
11	4.29	17 28 02.96	−14 25 08.5	1.42	5.6 ± 3.6	⋯
12	4.36	17 28 22.78	−14 21 24.9	1.18	8.6 ± 4.1	S53
13	4.68	17 28 21.94	−14 18 39.3	1.45	6.8 ± 3.8	⋯
14	4.86	17 27 59.90	−14 16 10.7	1.33	8.8 ± 4.1	⋯
15	5.63	17 28 11.56	−14 26 16.7	2.06	6.3 ± 3.8	⋯
16	6.12	17 28 19.78	−14 15 56.0	0.73	1472.6 ± 39.4	PDS 456
17	6.62	17 27 59.59	−14 14 23.6	2.89	6.4 ± 3.8	⋯
18	6.64	17 27 54.47	−14 27 01.4	2.77	6.8 ± 4.0	⋯
19	7.01	17 27 51.45	−14 14 40.6	2.70	8.3 ± 4.1	P388
20	7.08	17 28 15.57	−14 27 28.4	3.30	6.6 ± 4.0	⋯
21	9.48	17 27 46.00	−14 29 10.9	2.24	29.0 ± 6.6	⋯
22	11.11	17 27 53.58	−14 31 39.0	7.31	11.2 ± 5.0	⋯
23	11.49	17 28 06.94	−14 09 24.1	2.15	66.7 ± 9.7	⋯
24	12.64	17 28 15.81	−14 33 14.4	2.89	59.1 ± 9.1	⋯

Table 7
(Continued)

Source Number	θ[a] (′)	*Chandra* R.A. (J2000, h, m, s)	*Chandra* Decl. (J2000, degree, ′, ″)	Position Error[b] (″)	ACIS Counts[c]	Other Identification[d]
			ObsID 17248			
1	0.33	17 27 51.40	−14 14 40.0	0.74	9.8 ± 4.3	P388
2	2.13	17 27 59.49	−14 14 23.8	0.73	41.8 ± 7.5	*Gaia*
3	2.16	17 27 44.74	−14 12 47.0	0.80	9.8 ± 4.3	⋯
4	2.60	17 27 40.36	−14 15 03.3	0.82	10.8 ± 4.4	*Gaia*
5	2.72	17 28 01.95	−14 14 24.4	1.02	4.7 ± 3.4	⋯
6	2.80	17 28 02.03	−14 14 55.5	0.97	5.7 ± 3.6	*Gaia*
7	2.84	17 27 59.82	−14 16 10.0	0.90	7.7 ± 4.0	⋯
8	3.38	17 27 41.82	−14 11 47.0	1.18	4.8 ± 3.4	⋯
9	3.45	17 27 54.67	−14 11 04.4	1.11	5.8 ± 3.6	⋯
10	3.49	17 27 37.98	−14 12 45.9	1.01	7.7 ± 4.0	⋯
11	3.71	17 27 39.38	−14 16 53.0	0.80	28.6 ± 6.4	*Gaia*
12	3.89	17 27 41.29	−14 11 14.2	0.77	53.8 ± 8.4	⋯
13	4.03	17 28 06.86	−14 13 25.4	1.47	4.6 ± 3.4	⋯
14	4.03	17 28 02.48	−14 11 32.0	1.14	7.8 ± 4.0	⋯
15	4.35	17 28 06.12	−14 16 37.3	1.05	11.5 ± 4.6	P391
16	5.03	17 27 40.36	−14 10 01.4	1.81	5.7 ± 3.6	⋯
17	6.00	17 27 52.16	−14 08 23.8	1.78	9.4 ± 4.3	⋯
18	6.30	17 28 06.64	−14 09 24.9	0.93	61.3 ± 8.9	⋯
19	6.79	17 27 43.19	−14 20 55.5	2.72	7.4 ± 4.1	⋯
20	7.21	17 28 19.76	−14 15 56.6	0.76	928.1 ± 31.5	PDS 456
21	7.85	17 27 49.45	−14 22 14.0	6.02	4.6 ± 3.6	⋯
22	7.86	17 27 35.95	−14 21 23.4	7.68	3.6 ± 3.4	⋯
23	8.54	17 27 42.03	−14 06 06.8	2.85	14.2 ± 5.1	⋯
24	9.02	17 27 52.99	−14 05 23.3	3.54	12.9 ± 5.0	⋯
25	9.13	17 28 23.85	−14 18 44.1	4.58	9.9 ± 4.6	⋯
26	9.66	17 28 00.89	−14 05 03.0	3.49	16.4 ± 5.4	⋯
27	10.29	17 28 30.65	−14 17 53.6	5.54	11.8 ± 5.0	⋯
28	10.47	17 28 22.70	−14 21 25.7	4.13	17.5 ± 5.7	S53
29	11.53	17 28 25.54	−14 22 15.1	5.11	18.9 ± 6.0	⋯
			ObsID 18088			
1	0.09	20 23 12.49	+20 42 48.8	0.72	18.7 ± 5.4	P443
2	0.31	20 23 13.78	+20 42 45.3	0.72	18.7 ± 5.4	P443
3	0.68	20 23 13.01	+20 43 24.0	0.75	8.6 ± 4.1	*Gaia*
4	1.75	20 23 19.68	+20 42 16.1	0.88	4.6 ± 3.4	⋯
5	1.85	20 23 07.24	+20 41 20.1	0.89	4.7 ± 3.4	*Gaia*
6	1.97	20 23 13.17	+20 40 46.2	0.90	4.6 ± 3.4	⋯
7	2.22	20 23 21.09	+20 41 48.4	0.73	34.6 ± 7.0	⋯
8	2.30	20 23 12.72	+20 45 01.8	0.86	6.8 ± 3.8	⋯
9	2.52	20 23 06.50	+20 40 37.7	0.73	50.6 ± 8.2	WISE
10	2.60	20 23 22.50	+20 43 51.0	0.95	5.6 ± 3.6	⋯
11	2.64	20 23 21.69	+20 41 12.9	0.95	5.6 ± 3.6	⋯
12	2.86	20 23 21.89	+20 44 32.6	1.18	3.5 ± 3.2	⋯
13	2.91	20 23 00.05	+20 42 57.7	0.81	14.6 ± 5.0	⋯
14	2.98	20 23 02.39	+20 40 53.9	1.21	3.6 ± 3.2	⋯
15	3.11	20 23 23.31	+20 40 55.9	1.13	4.5 ± 3.4	⋯
16	3.14	20 23 08.38	+20 45 42.8	0.89	9.8 ± 4.3	*Gaia*
17	4.23	20 23 15.65	+20 46 53.7	1.14	8.7 ± 4.1	⋯
18	4.61	20 23 22.48	+20 38 45.6	1.29	8.1 ± 4.1	⋯
19	5.24	20 23 23.26	+20 38 08.4	1.71	6.9 ± 4.0	⋯
20	6.14	20 23 08.09	+20 36 40.5	0.95	49.0 ± 8.2	⋯
21	6.78	20 23 04.91	+20 49 16.7	2.59	7.9 ± 4.1	⋯
22	7.08	20 22 51.23	+20 47 46.7	2.13	11.7 ± 4.7	⋯
23	7.48	20 23 00.47	+20 49 39.5	2.43	11.6 ± 4.7	⋯
24	7.63	20 23 18.72	+20 35 14.2	0.96	115.4 ± 11.9	*Gaia*
25	7.87	20 23 18.04	+20 50 29.0	1.58	27.3 ± 6.5	⋯
26	7.91	20 23 45.35	+20 44 35.8	2.37	14.3 ± 5.1	⋯
27	8.27	20 22 49.82	+20 49 04.8	2.68	13.9 ± 5.1	⋯
28	8.47	20 23 18.46	+20 51 05.0	1.81	27.8 ± 6.6	⋯
29	9.50	20 23 50.97	+20 45 46.5	1.90	38.8 ± 7.5	⋯
30	12.62	20 23 30.75	+20 30 51.5	3.08	53.0 ± 9.0	⋯
31	15.20	20 23 07.27	+20 57 52.5	3.57	94.3 ± 13.4	⋯

Table 7
(Continued)

Source Number	θ[a] (′)	*Chandra* R.A. (J2000, h, m, s)	*Chandra* Decl. (J2000, degree, ′, ″)	Position Error[b] (″)	ACIS Counts[c]	Other Identification[d]
			ObsID 17245			
1	0.14	20 24 21.69	+33 50 50.3	0.72	15.5 ± 5.1	P448
2	0.24	20 24 23.33	+33 51 00.3	0.76	7.6 ± 4.0	P448
3	0.84	20 24 18.23	+33 50 48.8	0.78	6.5 ± 3.8	⋯
4	1.47	20 24 27.65	+33 51 51.7	0.75	13.6 ± 4.8	⋯
5	1.88	20 24 23.64	+33 49 04.0	0.83	6.7 ± 3.8	⋯
6	2.63	20 24 27.22	+33 48 30.6	0.86	8.7 ± 4.1	⋯
7	2.99	20 24 23.31	+33 53 54.4	0.81	15.4 ± 5.1	⋯
8	3.21	20 24 06.77	+33 50 47.9	1.19	4.3 ± 3.4	⋯
9	3.53	20 24 07.81	+33 52 47.3	0.97	9.2 ± 4.3	⋯
10	3.70	20 24 30.05	+33 47 35.7	1.12	6.6 ± 3.8	⋯
11	3.98	20 24 03.83	+33 52 02.0	0.71	714.1 ± 27.8	V404 Cyg
12	4.34	20 24 41.47	+33 49 13.8	1.18	8.4 ± 4.1	⋯
13	5.17	20 23 58.42	+33 52 25.6	1.15	14.5 ± 5.1	⋯
14	5.61	20 24 09.83	+33 55 54.7	1.53	10.0 ± 4.6	⋯
15	5.85	20 24 02.53	+33 55 06.5	1.67	9.7 ± 4.6	⋯
16	6.92	20 23 53.11	+33 54 18.0	1.05	51.3 ± 8.5	P445
17	6.95	20 24 42.95	+33 45 27.7	2.28	10.1 ± 4.6	⋯
18	8.57	20 24 56.80	+33 46 14.8	2.51	17.1 ± 5.7	⋯
19	8.68	20 23 59.22	+33 43 40.5	3.61	11.1 ± 5.0	⋯
20	9.31	20 23 39.69	+33 47 58.9	1.64	48.1 ± 8.3	P444
21	13.70	20 24 50.20	+33 38 31.2	8.44	19.5 ± 9.3	⋯
22	16.89	20 25 07.79	+33 36 56.1	5.16	84.9 ± 17.7	⋯
			ObsID 17704			
1	2.88	20 24 03.23	+33 49 03.7	1.10	4.3 ± 3.4	⋯
2	2.88	20 24 13.09	+33 54 25.6	1.07	4.5 ± 3.4	⋯
3	2.89	20 23 56.11	+33 53 29.9	0.89	8.5 ± 4.1	⋯
4	3.46	20 24 02.59	+33 55 07.3	0.95	9.4 ± 4.3	ObsID 17245
5	3.62	20 24 00.39	+33 48 29.3	0.78	40.0 ± 7.5	P446
6	3.80	20 23 55.67	+33 48 53.2	1.10	7.3 ± 4.0	⋯
7	3.86	20 23 53.23	+33 54 18.1	0.80	34.3 ± 7.0	P445
8	4.14	20 24 09.92	+33 55 54.4	1.14	8.2 ± 4.1	ObsID 17245
9	4.34	20 24 19.01	+33 55 25.0	1.73	4.2 ± 3.4	⋯
10	4.35	20 24 23.64	+33 49 03.8	1.18	8.6 ± 4.3	ObsID 17245
11	5.73	20 24 24.80	+33 56 15.1	1.47	11.4 ± 4.7	⋯
12	6.29	20 24 29.88	+33 47 35.4	1.75	11.1 ± 5.0	ObsID 17245
13	6.89	20 23 39.67	+33 48 00.8	1.25	29.0 ± 6.7	P444
14	7.00	20 23 51.52	+33 57 58.6	2.49	9.1 ± 4.6	⋯
15	7.01	20 24 28.73	+33 46 22.5	1.89	13.7 ± 5.5	⋯
16	7.02	20 23 39.70	+33 47 47.2	1.13	41.8 ± 7.8	P444
17	7.51	20 24 41.37	+33 49 13.7	4.16	6.1 ± 4.3	⋯
18	8.72	20 24 23.14	+33 59 53.3	6.53	5.9 ± 4.6	⋯
19	9.05	20 23 54.72	+33 43 09.0	4.34	10.2 ± 5.4	⋯
20	9.38	20 24 17.05	+34 00 58.3	7.70	6.2 ± 4.9	⋯
21	10.37	20 24 56.45	+33 49 50.1	8.49	7.7 ± 5.7	⋯
22	11.68	20 24 56.73	+33 46 11.6	3.99	27.0 ± 8.1	⋯
23	13.25	20 23 05.06	+33 48 58.7	7.15	20.8 ± 10.0	⋯
24	14.89	20 23 07.79	+33 43 32.1	7.26	31.4 ± 13.0	⋯
25	15.83	20 25 10.80	+33 43 01.3	1.64	722.9 ± 30.1	QSO B2023+336
			ObsID 18089			
1	0.31	21 19 35.52	+33 36 44.0	0.75	8.3 ± 4.1	P463
2	1.25	21 19 40.34	+33 37 31.5	0.91	3.2 ± 3.2	⋯
3	1.36	21 19 38.41	+33 35 52.6	0.79	7.3 ± 4.0	⋯
4	1.57	21 19 27.30	+33 37 01.0	0.93	3.4 ± 3.2	⋯
5	1.60	21 19 30.27	+33 38 18.1	0.84	5.3 ± 3.6	⋯
6	2.30	21 19 35.41	+33 34 42.8	0.85	7.2 ± 4.0	WISE
7	2.44	21 19 24.40	+33 35 54.1	0.77	19.3 ± 5.6	*Gaia*
8	2.45	21 19 42.69	+33 38 50.0	0.75	24.6 ± 6.1	*Gaia*
9	2.53	21 19 34.26	+33 39 32.2	0.76	21.6 ± 5.8	*Gaia*
10	2.60	21 19 36.87	+33 34 26.9	0.85	9.2 ± 4.3	⋯
11	2.77	21 19 35.66	+33 34 15.1	1.08	4.2 ± 3.4	⋯

Table 7
(Continued)

Source Number	θ[a] (′)	*Chandra* R.A. (J2000, h, m, s)	*Chandra* Decl. (J2000, degree, ′, ″)	Position Error[b] (″)	ACIS Counts[c]	Other Identification[d]
12	3.07	21 19 38.99	+33 34 03.7	1.07	5.1 ± 3.6	···
13	3.32	21 19 37.40	+33 40 17.3	1.03	6.6 ± 3.8	···
14	3.44	21 19 18.36	+33 36 50.9	0.80	25.0 ± 6.2	···
15	3.50	21 19 35.11	+33 33 31.1	0.97	8.9 ± 4.3	···
16	3.59	21 19 26.19	+33 33 54.8	0.79	30.9 ± 6.7	···
17	3.72	21 19 26.11	+33 40 15.2	0.85	18.5 ± 5.4	*Gaia*
18	3.95	21 19 17.11	+33 35 36.3	1.07	8.7 ± 4.3	···
19	4.23	21 19 29.13	+33 32 56.9	0.70	5212.5 ± 73.2	*Gaia*, LEDA 2034356
20	4.39	21 19 25.18	+33 33 06.8	1.10	10.4 ± 4.6	···
21	4.75	21 19 16.88	+33 34 05.1	1.26	9.2 ± 4.4	···
22	4.80	21 19 20.72	+33 33 13.5	1.28	9.2 ± 4.4	···
23	5.35	21 19 45.09	+33 32 06.2	1.54	8.6 ± 4.4	···
24	5.44	21 19 18.99	+33 32 41.2	1.61	8.4 ± 4.4	*Gaia*
25	5.94	21 19 52.83	+33 41 37.8	1.86	8.6 ± 4.3	···
26	7.38	21 19 28.76	+33 29 44.8	1.11	53.1 ± 8.5	WISE
27	7.87	21 19 49.72	+33 44 15.1	2.43	13.6 ± 5.2	···
28	7.91	21 19 26.22	+33 44 42.8	2.48	13.4 ± 5.2	···
29	7.97	21 19 56.19	+33 43 37.5	1.90	20.5 ± 6.0	···
30	8.03	21 20 07.13	+33 32 37.6	1.64	27.4 ± 6.6	···
31	8.27	21 19 46.35	+33 44 56.0	2.34	16.9 ± 5.7	···
32	8.49	21 19 25.96	+33 28 43.9	2.67	15.2 ± 5.6	···
33	8.54	21 19 51.59	+33 44 48.8	5.65	6.4 ± 4.4	···
34	9.08	21 20 06.88	+33 30 51.6	5.22	8.4 ± 4.9	···
35	9.44	21 20 16.71	+33 33 23.8	2.39	25.8 ± 6.7	···
36	9.63	21 20 17.15	+33 40 54.6	3.86	14.4 ± 5.7	···
37	9.64	21 19 53.64	+33 45 49.1	3.21	18.2 ± 6.1	···
38	9.82	21 19 41.80	+33 46 43.7	3.31	18.6 ± 6.2	···
39	10.03	21 19 58.01	+33 45 48.8	2.15	38.2 ± 7.9	···
40	10.16	21 19 14.17	+33 27 49.0	2.68	28.1 ± 7.2	···
41	10.53	21 19 47.83	+33 47 11.8	2.79	30.4 ± 8.3	···
42	10.86	21 20 26.90	+33 37 40.8	2.87	32.5 ± 7.7	···
43	11.09	21 20 17.76	+33 30 26.9	4.13	21.4 ± 6.9	···
44	11.52	21 19 30.56	+33 48 29.8	1.54	143.6 ± 14.3	···
45	11.79	21 20 30.35	+33 39 22.4	5.76	17.8 ± 6.8	···
46	12.39	21 20 21.43	+33 29 18.7	4.08	32.7 ± 8.2	···
47	13.45	21 20 34.64	+33 31 56.9	4.49	39.3 ± 9.2	···
			ObsID 18087			
1	0.15	13 03 23.94	−63 48 07.4	0.74	9.7 ± 4.3	···
2	0.49	13 03 28.57	−63 48 17.9	0.84	3.7 ± 3.2	···
3	1.65	13 03 27.01	−63 46 22.7	0.87	4.7 ± 3.4	VISTA
4	1.81	13 03 08.61	−63 47 49.7	0.88	4.6 ± 3.4	···
5	2.26	13 03 13.96	−63 49 55.7	0.90	5.6 ± 3.6	*Gaia*
6	2.47	13 03 46.92	−63 48 26.9	0.76	20.7 ± 5.7	*Gaia*
7	2.50	13 03 12.60	−63 45 55.4	0.93	5.6 ± 3.6	···
8	2.58	13 03 05.10	−63 49 23.6	0.88	7.6 ± 4.0	···
9	2.66	13 03 22.75	−63 45 22.1	0.79	15.6 ± 5.1	*Gaia*
10	2.66	13 03 01.26	−63 47 29.4	1.02	4.6 ± 3.4	VISTA
11	3.90	13 02 50.04	−63 47 23.1	1.20	6.3 ± 3.8	*Gaia*
12	4.63	13 02 47.63	−63 50 08.5	0.72	479.1 ± 22.9	*Gaia*, PSR B1259–63
13	6.55	13 04 20.28	−63 50 22.5	3.21	5.5 ± 3.8	···
14	6.65	13 03 51.08	−63 54 00.4	1.65	14.4 ± 5.1	···
15	8.89	13 02 09.13	−63 45 02.3	4.75	8.7 ± 4.7	···
16	10.39	13 02 12.71	−63 54 42.1	6.01	11.1 ± 5.3	···
17	13.87	13 01 58.66	−63 58 07.5	0.97	4084.0 ± 65.1	S43

Notes.
[a] The angular distance between the *Chandra* aimpoint and the source.
[b] The 90% confidence uncertainty on the position, including statistical and systematic contributions.
[c] The number of ACIS counts detected (after background subtraction) in the 0.5–7 keV band (except for ObsID 17704, for which the energy band is 2–7 keV). The errors are 68% confidence Poisson errors using the analytical approximations from Gehrels (1986).
[d] There is an entry in this column if the *Chandra* source may be identified with another source. The identifications may be names of *NuSTAR* serendips, names of known sources, or names of catalogs if we simply identified the *Chandra* source with a source in an optical or near-IR catalog.

Table 8
Position Shifts

ObsID	Matches	R.A. shift (arcsec)	Decl. shift (arcsec)
17246	…	…	…
17247	7	0.59 W	0.25 S
17248	4	0.10 E	0.36 S
18088	5	0.13 E	0.09 N
17245	1 (V404 Cyg)	…	…
17704	4 (X-ray)	0.45 E	0.26 S
18089	9	0.12 E	0.08 S
18087	8	0.10 W	0.16 S

ORCID iDs

John A. Tomsick https://orcid.org/0000-0001-5506-9855
George B. Lansbury https://orcid.org/0000-0002-5328-9827
Farid Rahoui https://orcid.org/0000-0001-7655-4120
James Aird https://orcid.org/0000-0003-1908-8463
David M. Alexander https://orcid.org/0000-0002-5896-6313
Maïca Clavel https://orcid.org/0000-0003-0724-2742
Francesca M. Fornasini https://orcid.org/0000-0002-9286-9963
Daniel Stern https://orcid.org/0000-0003-2686-9241

References

Ajello, M., Alexander, D. M., Greiner, J., et al. 2012, ApJ, 749, 21
Bird, A. J., Bazzano, A., Malizia, A., et al. 2016, ApJS, 223, 15
Casares, J. 2015, ApJ, 808, 80
Cox, A. N. 2000, Allen's Astrophysical Quantities (4th ed.; New York: AIP Press)
Freeman, P. E., Kashyap, V., Rosner, R., & Lamb, D. Q. 2002, ApJS, 138, 185
Gehrels, N. 1986, ApJ, 303, 336
Güver, T., & Özel, F. 2009, MNRAS, 400, 2050
Harrison, F. A., Craig, W. W., Christensen, F. E., et al. 2013, ApJ, 770, 103
Heinz, S., Corrales, L., Smith, R., et al. 2016, ApJ, 825, 15
Kalberla, P. M. W., Burton, W. B., Hartmann, D., et al. 2005, A&A, 440, 775
Krivonos, R. A., Tsygankov, S. S., Lutovinov, A. A., et al. 2015, ApJ, 809, 140
Lansbury, G. B., Stern, D., Aird, J., et al. 2017, ApJ, 836, 99
Lutovinov, A. A., Revnivtsev, M. G., Tsygankov, S. S., & Krivonos, R. A. 2013, MNRAS, 431, 327
Patterson, J. 1998, PASP, 110, 1132
Tomsick, J. A., Lansbury, G. B., Rahoui, F., et al. 2017, ApJS, 230, 25
Weisskopf, M. C. 2005, arXiv:astro-ph/0503091